Theor Chem Acc (2010) 127:539–550
DOI 10.1007/s00214-010-0743-5

REGULAR ARTICLE

How do phosphoramides compete with phosphine oxides in lanthanide complexation? Structural, electronic and energy aspects at ab initio and DFT levels

Khodayar Gholivand · Hamid Reza Mahzouni · Mehdi D. Esrafili

Received: 22 November 2009 / Accepted: 3 March 2010 / Published online: 21 March 2010

Abstract Novel comparison of the structural, electronic and energy aspects of lanthanide complexes of model phosphoramides (**PA**s) with those of phosphine oxides (**PO**s), phosphate esters (**PE**s) and phosphoryl trihalides (**PH**s) has been carried out by ab initio and DFT calculations. Atoms in Molecules (AIM) and Natural Bonding Orbital (NBO) analyses were performed to understand the electronic structure of ligands **L** and related complexes, **L**–Ln^{3+}. NBO analysis indicates that the negative charge on phosphoryl oxygen (O_P) and the *p* character of the phosphoryl lone pair, $Lp(O_P)$, increase in the order **PH** < **PE** < **PO** < **PA**. Positive charge of the lanthanide cation in **PA** complexes is less than those of **PH**, **PE** and **PO** complexes, due to the more intense ligand to metal charge transfer (LMCT). The metal–ligand distance decreases in the order **PH** > **PE** > **PO** > **PA**, which is confirmed by the results of AIM analysis. Charge density at the bond critical point of **L**–Ln^{3+} follows the sequence **PH** < **PE** < **PO** < **PA**. The results of the Energy Decomposition Analysis (EDA) indicate that the donative interaction and LMCT increases in order **PH** < **PO** < **PE** < **PA**. The effect of basis set superposition error (BSSE) on the **L**···Ln^{3+} interaction energies was also studied in detail at DFT, MP2 and CCSD(T) levels using the counterpoise (CP) method. Trends in the CP-corrected **L**–Ln^{3+} bond energies are in good accordance with the optimized O_P···Ln^{3+} distances. The results show that the difference between CP-corrected and uncorrected interaction energies in **PA** complexes is larger than those in the others, because **PA**s are more deformable. It is depicted that **PA**s are comparable with **PO**s in lanthanide complexation.

Keywords Lanthanide complex · DFT calculation · NBO · AIM · Phosphoramide · BSSE

K. Gholivand (✉) · H. R. Mahzouni · M. D. Esrafili
Department of Chemistry, Tarbiat Modares University, P.O. Box 14115-175, Tehran, Iran
e-mail: gholi_kh@modares.ac.ir

1 Introduction

Research aimed at designing the better extracting agents for rare earth cations is of interest in the nuclear waste management and also from a basic point of view [1–12]. It has been well documented that the phosphoryl containing ligands (phosphine oxides and phosphate esters) have potential to establish strong non-covalent interaction with oxophilic metals like lanthanides [13–18]. Such *O*-donor ligands are even better than the amide and pyridine derivatives to form lanthanide complex from the energy viewpoint [13, 14]. Gas phase calculations for small molecules lead to a better understanding of the reactions in solution [19, 20]. Thus, quantum mechanical (QM) calculations have previously been carried out to obtain some information about the binding features of neutral phosphoryl containing ligands to lanthanide and actinide cations [13–18, 21]. In this context, the effect of electron donation and polarizability of R (R = alkyl, aryl, alkoxy) on the R_3PO···Ln^{3+} interaction have been well studied [15, 16]. It is well known that the binding strength of the ligands is often in the linear correlation of their basicity [22, 23]. The latter is markedly dependent on the nature of phosphoryl substituents (R), polarization and charge transfer effects [16, 24]. Schurhammer et al. [15] have shown that the O_P···Ln^{3+} interaction energy decreases on going from alkyl to alkoxy substitution in R_3PO ligands, owing to the electron-withdrawing nature of the alkoxy groups.

Moreover, the long alkyl groups in lipophilic extractants, such as TOPO (tri-octyl phosphine oxide) and TBPO (tributyl phosphine oxide), play a key role in efficiently extraction of lanthanides [25].

Generally, phosphine oxides are prepared from several synthetic routes (Arbusov and Wittig reactions, oxidation of phosphines, *etc*.) using expensive reagents [26]. Therefore, research in the pursuit of finding the cost-effective extractant molecules remains to be investigated. The synthesis pathways of phosphoramides are relatively inexpensive with respect to the phosphine oxides [26]. A question that comes now to mind is that whether phosphoramides are good alternative for phosphine oxides in lanthanide complexation or not. To our knowledge, QM calculations on the structural, electronic and energy aspects of non-covalent interactions of lanthanide cations with phosphine oxides and phosphate esters have been extensively performed [13–16], but not with *phosphoramides*, $(NHR)_3PO$. To extend and develop these areas, we have decided to perform precise comparison of phosphoramides (**PA**s) with phosphine oxides (**PO**s), phosphate esters (**PE**s) and parent phosphoryl trihalides (**PH**s) as complexant agents. Hence, the small isoelectronic ligands of R_3PO type (group 1; R = CH_3, NH_2, OH and F, and group 2; R = CH_2Me, NHMe, OMe and Cl) were modeled as representatives for the aforementioned families. However, to save computer time, we did not consider the other ligands with longer alkyl chain.

Based on the Grimm's hydride shift rule [27], the chemical properties of isoelectronic ligands derived from $CH_3/NH_2/OH/F$ and also $CH_2Me/NHMe/OMe/Cl$ are expected to change gradually from the **PH**s to **PE**s, **PA**s and **PO**s in line with the electronegativity and polarization effects. The major aim of the present work is to study the trends in binding features of isoelectronic phosphoryl donors in lanthanide complexation. For this reason, we have analyzed the negative charge on the phosphoryl oxygen O_P, using the data of AIM and NBO calculations, to compare the intrinsic basicity and cation affinity of the ligands. The structural and energy aspects of the complexes were also studied for comparison of the $\mathbf{L}\cdots Ln^{3+}$ interaction energies in series of the ligands. The effect of cation size on the ligand binding strength was also investigated. To achieve this goal, La^{3+}, Eu^{3+} and Lu^{3+} were considered as large, average and small cations, respectively.

2 Computational details

DFT methods are able to describe the structure of lanthanide complexes in a quantitative manner [28]. Thus, geometries of the free ligands **L** and complexes $\mathbf{L}$–Ln^{3+} (Ln = La, Eu and Lu) were fully optimized in vacuum at B3LYP level. Whereas 4f electrons do not participate directly in Ln–ligand bonds [28, 29], 46 + $4f^n$ electrons of La^{3+}, Eu^{3+} and Lu^{3+} ions were modeled by quasirelativistic effective core potentials (ECPs) of the Stuttgart group [30, 31]. The Wipff research group has previously shown that the use of large core ECP is good enough for calculations on the $H_3PO\cdots Eu^{3+}$ system [16]. These ECPs with highly stabilized f orbitals treat $[Kr]4d^{10}4f^n$ as fixed cores, when n = 0, 6 and 14 for La^{3+}, Eu^{3+} and Lu^{3+}, respectively. The valence electrons were taken into account by the affiliated (7s6p5d)/[5s4p3d] basis set adding one f polarization function of exponent 0.591 [32]. The other atoms H, C, N, O, F, P and Cl were described by 6–31G* and 6–31 + G* standard basis sets. NBO and Natural Population Analyses (NPA) [33] were performed with the optimized geometries to investigate the charge distributions in the free ligands, **L**, and complexes, $\mathbf{L}$–Ln^{3+}, at B3LYP/6–31 + G* level of theory. Topological analysis of the electron density and its Laplacian was characterized by means of the Bader's Atoms in Molecules methodology [34, 35]. The AIM parameters of the free ligands and their complexes were calculated at B3LYP level and then compared together. The starting point for the AIM calculation is the electron density, ρ, which may be calculated from the many-electron single-determinant or many-determinant wave function obtained by a variety of theoretical methods. However, the electron density necessary for meaningful analysis by means of AIM must be obtained with a basis set flexible enough for an accurate representation of the bonding regions. For heavy atoms, which usually necessitates the use of ECP, it is necessary to treat the valence shell and at least one sub-valence shell explicitly to obtain meaningful results from the integrations. It is important to note that bond paths cannot be traced to the nuclei of atoms described by ECPs [36]. For the AIM calculations of Ln^{3+}–ligand systems, the aforementioned ECPs and related basis sets for Ln^{3+} ions and 6–31 + G* basis set for the other atoms were used. The similar scheme has been also considered for calculation of the NBO and energies. Binding energies were calculated using DFT, MP2 and CCSD(T) methods. Although DFT methods usually overestimate the metal–ligand binding energy [37, 38], but the overestimation is even more pronounced with the MP2 method [39–41]. Thus, geometries of complexes have been optimized at B3LYP level and then compared with MP2 geometries. For both of methods, the optimized geometries at 6–31 + G* were used to calculate the interaction energies (ΔEs) between the ligands and cations Ln^{3+}. The interaction energies have been calculated by using supermolecular approach [42] at 6–311 ++ G**. Furthermore, the DFT geometries were used to calculate CCSD(T) interaction energies at 6–311 ++ G**. The $\mathbf{L}'$–Ln^{3+} bond energies and fully dissociation energies of all complexes have been

computed when $\mathbf{L}'$ is a deformed ligand in complex coordinate. The interaction energies have been corrected for basis set superposition error (BSSE) by using the Boys-Bernardi counterpoise (CP) method [43]. All quantum chemical calculations have been carried out using the Gaussian 98 package [44]. Furthermore, based on the Morokuma approach [45, 46], an energy decomposition analysis (EDA) has been carried out to get a more detailed insight into the nature of the metal–ligand interaction using GAMESS package [47].

3 Results and discussions

The general structure of model ligands and resulting complexes are represented in Fig. 1. Since the trends of the structural parameters and energy terms are not dependent of the computational level, the B3LYP values are discussed in the paper. Whereas, the large ECPs were used for all metal ions, the standard basis sets 6–31G*, 6–31 + G*, 6–311 + G* and 6–311 ++ G** are only noted for simplicity in the text, which refer to the main group elements. In this section, we first compare the structural parameters of the free ligands in series of Me/NH_2/OH/F and also of CH_2Me/NHMe/OMe/Cl. In the following, the charge analyses and cation affinities of the ligands are also discussed.

3.1 Structural parameters of the free ligands and complexes

The structural parameters and dipole moment of the optimized free ligands at B3LYP level are presented in Table 1. These parameters are changed gradually from phosphoryl trihalides to trialkylphosphine oxide. For instance, d(P = O) increases from 1.458 Å in F_3PO to 1.506 Å in Me_3PO. Similar trends are also observed in series of CH_2Me/NHMe/OMe/Cl ligands. The P–X (X = C, N, O and F) bond lengthens from phosphoryl halides to alkylphosphine oxide due to the decrease in electronegativity of atom X [48]. The geometries of the free ligands are slightly changed on going from the small basis set 6–31G* to 6–311 + G* and 6–311 ++ G**. These changes account for the variation of dipole moment values from the small to large basis sets. Dobado et al [49] have previously shown that the P = O bond lengthens with decrease in the electrostatic attraction between the phosphorus and oxygen atoms, giving the higher dipole moment. This is clearly seen in the model ligands ongoing from phosphoryl halides to phosphine oxides, as represented in Table 1. However, the computational level has no effect on the trends in geometrical and electronic properties.

The P = O bond lengthens markedly when the ligand is coordinated (by about 0.2 to 0.3 Å). This is consistent with decrease in electron density between phosphorus and oxygen atoms in complexes compared with free ligands (see Sect. 3.2). The P = O bond length is 1.727, 1.729,

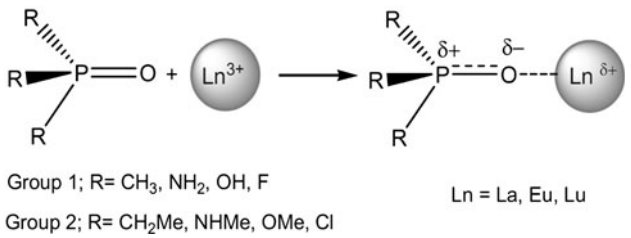

Fig. 1 Illustration of the structure of isoelectronic model ligands and resulting lanthanide complexes

Table 1 Selected optimized parameters in free ligands **L** at B3LYP level

Ligand	Basis set			
	6–31G*	6–31 + G*	6–311 + G*	6–311 ++ G**
d(P = O)/Å				
Me_3PO	1.501	1.506	1.500	1.500
$(NH_2)_3PO$	1.489	1.491	1.486	1.485
$(OH)_3PO$	1.473	1.476	1.469	1.469
F_3PO	1.456	1.458	1.450	1.450
$(CH_2Me)_3PO$	1.505	1.510	1.505	1.505
$(NHMe)_3PO$	1.491	1.495	1.490	1.490
$(OMe)_3PO$	1.475	1.479	1.473	1.473
Cl_3PO	1.472	1.472	1.465	1.465
d_{avg}(P–X)[a]/Å				
Me_3PO	1.835	1.835	1.830	1.830
$(NH_2)_3PO$	1.690	1.689	1.682	1.682
$(OH)_3PO$	1.616	1.616	1.610	1.611
F_3PO	1.559	1.566	1.562	1.562
$(CH_2Me)_3PO$	1.851	1.853	1.848	1.848
$(NHMe)_3PO$	1.687	1.689	1.683	1.683
$(OMe)_3PO$	1.610	1.610	1.606	1.606
Cl_3PO	2.039	2.039	2.040	2.041
Dipole moment (Debye)				
Me_3PO	4.284	4.650	4.652	4.639
$(NH_2)_3PO$	3.473	4.312	4.362	4.314
$(OH)_3PO$	3.394	3.355	3.518	3.373
F_3PO	1.682	1.583	1.496	1.496
$(CH_2Me)_3PO$	4.401	4.846	4.827	4.845
$(NHMe)_3PO$	3.938	4.216	4.261	4.233
$(OMe)_3PO$	3.644	3.832	3.858	3.869
Cl_3PO	2.013	2.271	2.286	2.286

[a] X = C, N, O and F atoms

1.637 and 1.587 Å in series of $(Me/NH_2/OH/F)_3PO$–La^{3+} complexes. These values amount to 1.750, 1.783, 1.682 and 1.671 Å, respectively, in series of CH_2Me analogues. The P = O bond elongation was intensified by electron donating capacity of the ligands owing to the stronger metal–ligand interaction. This agrees with decrease of $O_P\cdots Ln^{3+}$ distance from $Me/NH_2/OH/F$ series of ligands to CH_2Me/NHMe/OMe/Cl ones (Table 2). The $O_P\cdots Ln^{3+}$ distance decreases in the order La > Eu > Lu due to the cation hardness effect. Table 2 shows that the P = O bond elongation is more intense with hardest cation (Lu^{3+}), as a function of metal–ligand distance.

It is noteworthy that the $O_P\cdots Ln^{3+}$ distance in **PA**–Ln^{3+} complexes is shorter than that in **PO** ones. It is 2.053 and 2.049 Å in Me_3PO–La^{3+} and $(NH_2)_3PO$–La^{3+} complexes, respectively. This difference is more sensible when the electron donation ability of ligands is increased. Table 2 shows that the $O_P\cdots Ln^{3+}$ distance decreases in the order of **PH** > **PE** > **PO** > **PA**. Thus, the non-covalent **PA**–Ln^{3+} interactions are expected to be stronger than those in the others that will be described in detail in the following sections.

3.2 AIM analysis

Based on the AIM theory, $\rho(r)$ and its Laplacian ($\nabla^2\rho$) at the bond critical point (bcp) provide information about the strength and characteristic of the bond between the two atoms. Laplacian of ρ is calculated as $\nabla^2\rho = \lambda_1 + \lambda_2 + \lambda_3$, when λ_i is Hessian eigenvalue of the charge density. The large values of ρ and the values of $\nabla^2\rho < 0$, $|\lambda_1|/\lambda_3 > 1$ and $|\lambda_2|/\lambda_3 > 1$ are calculated for shared interactions or covalent bonds. On the contrary, the small values of ρ and the values of $\nabla^2\rho > 0$, $|\lambda_1|/\lambda_3 < 1$ and $|\lambda_2|/\lambda_3 < 1$ correspond to closed-shell interactions (ionic, hydrogen bond, van der Waals bonds) [34, 35].

The AIM atomic charges of phosphoryl oxygen atoms; $q(O_P)$, charge density (ρ) and its Laplacian ($\nabla^2\rho$) at the P = O bcp and also at bcp of the $O_P\cdots Ln^{3+}$ interactions were calculated and summarized in Tables 3 and 4. The

Table 2 Selected optimized parameters in charged complexes **L**–Ln^{3+} at B3LYP/6–31 + G* and MP2/6–31 + G* levels

Cation	Ligand	$d(M^{3+}\cdots O_P)$/Å		$d(P=O)$/Å		$d_{avg}(P–X)$/Å	
		B3LYP	MP2	B3LYP	MP2	B3LYP	MP2
La^{3+}	Me_3PO	2.053 (2.051)	2.053	1.727 (1.727)	1.730	1.801 (1.802)	1.782
	$(NH_2)_3PO$	2.049 (2.047)	2.046	1.729 (1.730)	1.732	1.616 (1.615)	1.611
	$(OH)_3PO$	2.082 (2.080)	2.084	1.637 (1.638)	1.636	1.548 (1.548)	1.550
	F_3PO	2.161 (2.157)	2.170	1.585 (1.587)	1.582	1.510 (1.509)	1.510
	$(CH_2Me)_3PO$	2.037 (2.036)	2.035	1.750 (1.752)	1.756	1.826 (1.825)	1.799
	$(NHMe)_3PO$	2.027 (2.025)	2.020	1.783 (1.786)	1.794	1.615 (1.614)	1.608
	$(OMe)_3PO$	2.043 (2.042)	2.042	1.682 (1.684)	1.681	1.539 (1.539)	1.542
	Cl_3PO	2.092 (2.090)	2.092	1.671 (1.673)	1.669	1.958 (1.957)	1.934
Eu^{3+}	Me_3PO	1.961 (1.959)	1.960	1.743 (1.744)	1.747	1.800 (1.800)	1.782
	$(NH_2)_3PO$	1.957 (1.954)	1.953	1.754 (1.756)	1.759	1.613 (1.612)	1.608
	$(OH)_3PO$	1.986 (1.983)	1.986	1.651 (1.654)	1.651	1.545 (1.546)	1.546
	F_3PO	2.053 (2.049)	2.060	1.598 (1.601)	1.595	1.507 (1.507)	1.509
	$(CH_2Me)_3PO$	1.947 (1.946)	1.945	1.768 (1.770)	1.775	1.825 (1.825)	1.798
	$(NHMe)_3PO$	1.937 (1.934)	1.929	1.816 (1.822)	1.851	1.613 (1.612)	1.605
	$(OMe)_3PO$	1.952 (1.949)	1.949	1.701 (1.706)	1.703	1.536 (1.535)	1.538
	Cl_3PO	1.992 (1.990)	1.992	1.689 (1.691)	1.689	1.955 (1.954)	1.931
Lu^{3+}	Me_3PO	1.880 (1.879)	1.883	1.753 (1.754)	1.753	1.799 (1.799)	1.781
	$(NH_2)_3PO$	1.876 (1.874)	1.877	1.767 (1.770)	1.768	1.611 (1.611)	1.607
	$(OH)_3PO$	1.900 (1.898)	1.903	1.660 (1.664)	1.659	1.543 (1.543)	1.544
	F_3PO	1.957 (1.955)	1.965	1.607 (1.609)	1.604	1.506 (1.506)	1.507
	$(CH_2Me)_3PO$	1.869 (1.868)	1.871	1.779 (1.781)	1.780	1.824 (1.823)	1.797
	$(NHMe)_3PO$	1.857 (1.858)	1.858	1.869 (1.839)	1.862	1.610 (1.610)	1.604
	$(OMe)_3PO$	1.871 (1.870)	1.873	1.712 (1.716)	1.710	1.534 (1.534)	1.537
	Cl_3PO	1.905 (1.904)	1.908	1.702 (1.705)	1.699	1.953 (1.952)	1.929

The values in parenthesis refer to the 6–31G* basis set

X = C, N, O and F atoms

value of $\nabla^2\rho$ at P = O bcp decreases from 1.771 au in F_3PO to 1.428 au in Me_3PO. This is in line with decrease of ionic contribution of P^+–O^- bond in series of **PH/PE/PA/PO** ligands. Decrease of the electronegativity in the order of F > O > N > C leads to the decrease of positive charge on phosphorus atom from **PH**s to **PE**, **PA** and **PO** analogues. As shown in Table 3, the values of ρ and $\nabla^2\rho$ at the P = O bcp are gradually decreased from **PH**s (0.242 au in F_3PO) to (0.215 au in Me_3P = O) in line with decrease of the P = O bond strength. But, similar trend is not observed in the case of the negative charge localized on phosphoryl O_P oxygen (**PA > PO > PE > PH**, Table 3). The O_P atoms are more negatively charged in $(NH_2)_3PO$ (−1.492 e^-) and $(NHMe)_3PO$ (−1.493 e^-) when compared to those of their analogues. Thus, **PA**s are expected to be more potent for cation binding. Similar trend is obtained for the $|\lambda_1|/\lambda_3$ values at P = O bcp. The precise assessment of the ionic and covalent contributions of the metal–ligand interaction is difficult. But, the small $|\lambda_1|/\lambda_3$ values in Table 3 reveal a charge separation in the respective atomic basins (P and O atoms). The AIM charge of phosphorus atom markedly increases from **PO**s to **PH**s (Table 3). This supports a partial ionic contribution in the P^+–O^- bond which generally strengthens by increase in the electronegativity of the substituents.

The charge density at the P = O bcp decreases when the ligands are coordinated to the metal cation (Tables 3 and 4). For instance, the ρ values at the P = O bcp are 0.215 and 0.128 au in Me_3PO and $Me_3PO\cdots La^{3+}$, respectively, which is in accordance with the lengthening of P = O upon complexation. Analysis of the obtained bond critical points for $O_P\cdots Ln^{3+}$ interactions, suggests a closed-shell interaction and ionic character of $O_P\cdots Ln^{3+}$. Hessian eigenvalues (λ_1, λ_2 and λ_3) of the charge density at the main bcp of the complexes are presented in Table 4. The values of $\nabla^2\rho > 0$ and $|\lambda_1|/\lambda_3 = |\lambda_2|/\lambda_3 = 0.204$ at the bcp of $O_P\cdots La^{3+}$ confirm the presence of ionic Me_3P = O···La^{3+} interaction. The values of $|\lambda_1|/\lambda_3$ and $|\lambda_2|/\lambda_3$ are increased in **PA**–Ln^{3+} complexes, and drop significantly in the cases of **PE** and **PH** complexes. For a given ligand, Laplacian of ρ at **L**···Ln^{3+} bcp increases in the order La < Eu < Lu. For instance, the magnitude of (ρ/Laplacian) at the $O_P\cdots La^{3+}$ bcp is (0.120/0.429 au) in Me_3PO–La^{3+} complex, which is increased in the cases of Me_3PO–Eu^{3+} (0.134/0.545 au) and Me_3PO–Lu^{3+} (0.141/0.673 au) complexes (Table 4). The ionic character and strength of $O_P\cdots Ln^{3+}$ interaction follow the cation hardness. This is confirmed by the shortening of the $O_P\cdots Ln^{3+}$ distance as $La^{3+} > Eu^{3+} > Lu^{3+}$.

The ρ values at the bcp of $O_P\cdots Ln^{3+}$ are 0.120/0.122 au in La^{3+} complexes of Me/NH_2 ligands, which amount to 0.134/0.136 au and 0.141/0.143 au in related Eu^{3+} and Lu^{3+} complexes, respectively. The charge density at the $(NH_2)_3PO\cdots Ln^{3+}$ bcps are more concentrated than those at $Me_3PO\cdots Ln^{3+}$ ones. This may explain the decrease of $O_P\cdots Ln^{3+}$ distance from **PO**–Ln^{3+} to **PA**–Ln^{3+} complexes (Tables 2 and 4). However, the charge density at the bcp of $(NH_2)_3PO\cdots La^{3+}$ is very close to that of $Me_3PO\cdots La^{3+}$ and decreases on going to $(OH)_3PO$ and F_3PO complexes. Similar results are obtained for $CH_2Me/NHMe/OMe/Cl$ ligands and also in **L**–Eu^{3+} and **L**–Lu^{3+} complexes.

3.3 NBO analysis

The factors that affect the bonding and electronic features of P = O group, are discussed in the following;

(i) The standard discussion of the P = O bond can be described in term of a combination of two different mesomeric forms [P^+–O^- ↔ P = O]. In this case, the electrostatic interaction between phosphorus and oxygen atoms generates a polar bond which overlaps with σ bond P–O [48]. A significant increase in positive charge on the phosphorus atom, q(P), strengthens the P = O bond in line with increase of the electronegativity and σ-acceptor character of the substituents X in the order C < N < O < F. Moreover, the appropriate acceptor orbital for the X_3P moiety of F_3P = O is at significantly lower energy than that in the others. Thus, the negative hyperconjugation π(P = O) → σ^*(P–X) is intensified in line with increase of the electronegativity from alkyl to halide substituents, which is accompanied by

Table 3 AIM parameters of P = O bond in free ligands at B3LYP/6–31 + G* level

Species	$q(O_P)^a$	q(P)	ρ(P = O)^b	$\nabla^2\rho$(P = O)^b	$\lvert\lambda_1\rvert/\lambda_3$ at P = O bcp
Me_3PO	−1.480	+3.127	0.215	1.428	0.168
$(NH_2)_3PO$	−1.492	+3.544	0.224	1.532	0.171
$(OH)_3PO$	−1.469	+3.657	0.233	1.644	0.166
F_3PO	−1.407	+3.740	0.242	1.771	0.160
$(CH_2Me)_3PO$	−1.485	+2.999	0.214	1.397	0.170
$(NHMe)_3PO$	−1.493	+3.522	0.222	1.507	0.172
$(OMe)_3PO$	−1.471	+3.649	0.231	1.619	0.167
Cl_3PO	−1.370	+2.646	0.230	1.695	0.156

[a] AIM atomic charge of phosphoryl O_P oxygen

[b] The values are reported in au

Table 4 Calculated main bcp parameters of the complexes at B3LYP/6–31 + G* level

Cation	Ligand	ρ (in au)		$\nabla^2\rho$ (in au)		$\lvert\lambda_1\rvert/\lambda_3$	
		P = O	$Ln^{3+}\cdots O_P$	P = O	$Ln^{3+}\cdots O_P$	P = O	$Ln^{3+}\cdots O_P$
La^{3+}	Me_3PO	0.128	0.120	0.375	0.429	0.240	0.204
	$(NH_2)_3PO$	0.132	0.122	0.335	0.427	0.263	0.206
	$(OH)_3PO$	0.160	0.111	0.672	0.417	0.224	0.199
	F_3PO	0.180	0.091	0.913	0.373	0.205	0.188
	$(CH_2Me)_3PO$	0.122	0.126	0.308	0.432	0.250	0.208
	$(NHMe)_3PO$	0.119	0.130	0.182	0.428	0.311	0.216
	$(OMe)_3PO$	0.145	0.123	0.492	0.432	0.241	0.210
	Cl_3PO	0.148	0.108	0.522	0.415	0.229	0.194
Eu^{3+}	Me_3PO	0.124	0.134	0.334	0.545	0.246	0.200
	$(NH_2)_3PO$	0.125	0.136	0.269	0.544	0.278	0.203
	$(OH)_3PO$	0.155	0.124	0.617	0.530	0.230	0.196
	F_3PO	0.175	0.104	0.843	0.469	0.211	0.188
	$(CH_2Me)_3PO$	0.118	0.139	0.266	0.552	0.259	0.204
	$(NHMe)_3PO$	0.112	0.145	0.116	0.551	0.348	0.211
	$(OMe)_3PO$	0.139	0.137	0.429	0.553	0.250	0.202
	Cl_3PO	0.142	0.122	0.457	0.521	0.237	0.194
Lu^{3+}	Me_3PO	0.120	0.141	0.314	0.673	0.248	0.189
	$(NH_2)_3PO$	0.122	0.143	0.240	0.674	0.286	0.191
	$(OH)_3PO$	0.151	0.132	0.586	0.649	0.233	0.188
	F_3PO	0.171	0.113	0.799	0.570	0.214	0.184
	$(CH_2Me)_3PO$	0.115	0.146	0.247	0.685	0.262	0.191
	$(NHMe)_3PO$	0.103	0.153	0.034	0.688	0.441	0.197
	$(OMe)_3PO$	0.135	0.144	0.402	0.687	0.253	0.191
	Cl_3PO	0.139	0.131	0.417	0.640	0.242	0.186

shortening of P = O bond [48]. This leads to the decrease in negative charge localized on O_P atom, $q(O_P)$, as C > N > O > F.

(ii) The charge transfer to the phosphoryl group is attenuated with decrease in π-donor character of the substituents in the order NHMe > NH_2 > OMe > OH > Me > F. Bollinger et al. have shown that the highly delocalized electronic cloud allows for the highly stabilized $(RN)_3P=O\cdots H^+$ system with respect to the $R_3P=O\cdots H^+$ [50]. Furthermore, the higher proton affinity of **PA**s simply correlates with negative charge on O_P atom, $q(O_P)$ [15].

It seems that factor (ii) in **PA**s is more important than that in the others, which may explain why $q(O_P)$ is more negative than that expected in **PA**s. The calculated NBO charges in Table 5 show that $q(O_P)$ is −1.100, −1.100, −1.074 and −1.018 in Me/NH_2/OH/F ligands, respectively. Similar results were obtained in CH_2Me/NHMe/OMe/Cl.

Natural electron configuration of O_P atom includes more electronic population in 2p orbital in Me_3PO ($2s^{1.81}2p^{5.27}$) and $(NH_2)_3PO$ ($2s^{1.82}2p^{5.26}$) and decreases in the cases of $(OH)_3PO$ ($2s^{1.81}2p^{5.22}$) and F_3PO ($2s^{1.81}2p^{5.15}$). The same trends obtained for CH_2Me/NHMe/OMe/Cl ligands (Table 5). The hybridization of $Lp(O_P)$ is $sp^{0.48}$ and $sp^{0.49}$ in Me_3PO and $(NH_2)_3PO$, respectively, and has less p character in $(OH)_3PO$ and F_3PO (Table 5). These confirm the higher basic potential of **PO**s and **PA**s when compared with **PE**s and **PH**s. The p character of $Lp(O_P)$ is slightly increased in CH_2Me analogues because of the electron donation of the additional alkyl group.

We also notice that the $O_P\cdots Ln^{3+}$ bonds have mostly $p^{1.00}$ or $p^{0.99}d^{0.01}$ hybridization in all complexes studied here. The hybridization of O_P in P = O bond varies from $sp^{2.01}$ in Me_3PO and $(NH_2)_3PO$ to $sp^{3.65}d^{0.02}$ and $sp^{2.75}d^{0.03}$ in $(OH)_3PO$ and F_3PO, respectively. Table 5 shows that the p character of P = O bond increases from **PO**s and **PA**s to **PE**s and **PH**s. It seems that the availability of lone pairs of phosphoryl oxygen, $Lp(O_P)$, in **PE**s and **PH**s are decreased for donation to the metal cation, due to the more participation in P = O π bonding.

The O_P atomic charge becomes more negative when the ligand is coordinated. The cation electrostatic filed pulls

Table 5 NBO parameters of the free ligands **L** at B3LYP/6–31 + G* level

Species	Atomic charges		NEC[a] of O_P	Hybridization	
	q(Op)	q(P)		O_P in P = O bond	Lone pair of O_P
Me_3PO	−1.100	+1.930	[core] $2s^{1.81}$ $2p^{5.27}$	$sp^{2.01}d^{0.01}$	$sp^{0.48}$
$(NH_2)_3PO$	−1.100	+2.334	[core] $2s^{1.82}$ $2p^{5.26}$	$sp^{2.01}d^{0.02}$	$sp^{0.49}$
$(OH)_3PO$	−1.074	+2.555	[core] $2s^{1.83}$ $2p^{5.22}$	$sp^{3.65}d^{0.02}$	$sp^{0.44}$
F_3PO	−1.018	+2.663	[core] $2s^{1.84}$ $2p^{5.15}$	$sp^{2.75}d^{0.03}$	$sp^{0.36}$
$(CH_2Me)_3PO$	−1.109	+1.964	[core] $2s^{1.81}$ $2p^{5.28}$	$sp^{1.98}d^{0.02}$	$sp^{0.50}$
$(NHMe)_3PO$	−1.109	+2.397	[core] $2s^{1.81}$ $2p^{5.27}$	$sp^{1.92}d^{0.02}$	$sp^{0.52}$
$(OMe)_3PO$	−1.081	+2.614	[core] $2s^{1.82}$ $2p^{5.23}$	$sp^{2.50}d^{0.02}$	$sp^{0.47}$
Cl_3PO	−0.977	+1.590	[core] $2s^{1.82}$ $2p^{5.13}$	$sp^{2.20}d^{0.02}$	$sp^{0.45}$

[a] Natural electron configuration of phosphoryl O_P oxygen

the charge density from the phosphoryl substituents to the coordinating site (O_P). The negative charge on the O_P atom is −1.100 in both of Me_3PO and $(NH_2)_3PO$, which is increased in the cases of Me_3PO–La^{3+} (−1.377) and $(NH_2)_3PO$–La^{3+} (−1.389), as represented in Table 6. This indicates that the polarization effect in **PA** complexes is slightly more than that in the others.

The positive charge of the lanthanide cation in the range of +2.5 to +2.9 suggests the ionic metal–ligand interaction [28]. The calculated natural charge of the lanthanide cations, q(M), are listed in Table 6 for all La, Eu and Lu complexes. The charge of the cation is +2.873, +2.818, +2.768 and +2.759 for La^{3+} complexes of (F/OH/Me/NH_2)$_3$PO. The lower positive charge of La^{3+} (+2.759) explains the higher degree of LMCT in $(NH_2)_3PO\cdots La^{3+}$ complex. These values decrease more with increasing charge donation ability in series of Cl/OMe/CH_2Me/NHMe ligands and with the cation hardness in the cases of Eu and Lu complexes.

The natural charge analysis of lanthanide cations reveals charge transfer from Lp(O_P) to unoccupied 5d orbital of metal cation [Lp(O_P) → 5d(metal)]. Table 6 shows that, the electronic populations in metal 5d orbitals are [core]5d(0.13/0.19/0.24/0.25) for (F/OH/Me/NH_2)$_3$PO–La^{3+} complexes. This electronic population increases with increasing of the electron donating nature of the phosphoryl substituents (Cl < OMe < CH_2Me < NHMe), and also with increase of the cation hardness (Table 6).

These confirm the higher degree of LMCT in **PA** complexes. The quantitative aspects of the hybridization of Lp(O_P), electron donation ability of the ligands and LMCTs suggest the strongest $O_P\cdots Ln^{3+}$ interaction in **PA** complexes.

3.4 Interaction energy

The uncorrected cation—ligand interaction energy can be estimated from the energy difference between the complex

Table 6 NBO parameters of the **L**–Ln^{3+} complexes at B3LYP/6–31 + G* level

Cation	Ligand	Atomic charges			NEC[a] of metal 5d orbital
		q(M)	q(Op)	q(P)	
La^{3+}	Me_3PO	2.768	−1.377	1.898	$5d^{0.24}$
	$(NH_2)_3PO$	2.759	−1.389	2.403	$5d^{0.25}$
	$(OH)_3PO$	2.818	−1.381	2.708	$5d^{0.19}$
	F_3PO	2.873	−1.376	2.874	$5d^{0.13}$
	$(CH_2Me)_3PO$	2.737	−1.373	1.927	$5d^{0.28}$
	$(NHMe)_3PO$	2.710	−1.386	2.426	$5d^{0.30}$
	$(OMe)_3PO$	2.769	−1.381	2.749	$5d^{0.24}$
	Cl_3PO	2.810	−1.376	1.456	$5d^{0.20}$
Eu^{3+}	Me_3PO	2.766	−1.392	1.891	$5d^{0.29}$
	$(NH_2)_3PO$	2.751	−1.405	2.395	$5d^{0.30}$
	$(OH)_3PO$	2.813	−1.397	2.709	$5d^{0.24}$
	F_3PO	2.869	−1.392	2.874	$5d^{0.17}$
	$(CH_2Me)_3PO$	2.741	−1.393	1.920	$5d^{0.32}$
	$(NHMe)_3PO$	2.703	−1.407	2.416	$5d^{0.35}$
	$(OMe)_3PO$	2.761	−1.402	2.746	$5d^{0.29}$
	Cl_3PO	2.805	−1.394	1.444	$5d^{0.24}$
Lu^{3+}	Me_3PO	2.609	−1.247	1.894	$5d^{0.39}$
	$(NH_2)_3PO$	2.599	−1.267	2.397	$5d^{0.40}$
	$(OH)_3PO$	2.684	−1.283	2.716	$5d^{0.31}$
	F_3PO	2.774	−1.318	2.882	$5d^{0.22}$
	$(CH_2Me)_3PO$	2.568	−1.233	1.924	$5d^{0.43}$
	$(NHMe)_3PO$	2.524	−1.255	2.416	$5d^{0.47}$
	$(OMe)_3PO$	2.609	−1.265	2.756	$5d^{0.39}$
	Cl_3PO	2.674	−1.275	1.432	$5d^{0.32}$

[a] Natural electron configuration

(ML) and its subunits (M and L) [42, 51] as defined in Eq 1;

$$\Delta E_{\text{uncorrected}} = E^{ML}_{ML}(ML) - E^{L}_{L}(L) - E^{M}_{M}(M) \quad (1)$$

where $E^{A}_{B}(C)$ is the electronic energy of molecular system C at geometry B computed with basis set A. In the

supermolecular approach, the basis set superposition error (BSSE) leads to overestimation of interaction energies, because the subunits utilize the basis sets of the partners [52, 53]. Generally, to avoid this problem, the results are corrected for BSSE. Based on counterpoise method, the CP-corrected interaction energy is calculated from Eq 2 [43].

$$\Delta E_{CP-corrected} = E^{ML}_{ML}(ML) - E^{ML}_{ML}(L) - E^{ML}_{ML}(M) \quad (2)$$

The energy difference between CP-corrected and uncorrected interaction energy is related to BSSE. The BSSE decrease significantly by considering deformation energies of the ligands [54]. It should be noted that free ligand, **L**, is deformed to **L′** upon complexation. Deformation energy can be estimated from Eq 3;

$$\Delta E_{deformation} = E^{L}_{ML}(L) - E^{L}_{L}(L) \quad (3)$$

Furthermore, the CP-corrected interaction energies are more lively description of complexation process from the energy viewpoint, when the deformation energy terms are taken into account. The complete CP-corrected interaction energy can be calculated from Eq 4, by consideration of the geometrical deformation [51, 54].

$$\Delta E_{GCP} = E^{ML}_{ML}(ML) - E^{ML}_{ML}(L) - E^{ML}_{ML}(M) + \Delta E_{deformation}(L) + \Delta E_{deformation}(M) \quad (4)$$

Based on Eqs 1–4, we have computed the uncorrected, CP-corrected and complete corrected interaction energies of our systems. The cation–ligand interaction energies (ΔE) are presented in Table 7. The uncorrected cation–ligand attraction energy ($-\Delta E_{uncorrected}$) increases from 138.8 in F_3PO–La^{3+} to 249.5 kcal mol^{-1} in $(NHMe)_3PO$–La^{3+}. This range shifts to 156.4–275.2 and 174.8–298.5 kcal mol^{-1} for corresponding Eu^{3+} and Lu^{3+} complexes, respectively, due to the cation hardness effect. Uncorrected attraction energies of Me–, NH_2–, OH– and F-substituted complexes of La^{3+} cation are 230.7, 229.7, 200.5, 138.8 kcal mol^{-1}, respectively. For a given cation, the uncorrected attraction energy of **PA**s is very close to that of **PO**s and decreases significantly in the order **PO** ≈ **PA** > **PE** > **PH**.

CP-corrected attraction energies are considerably different from the uncorrected ones and follow the sequence **PA** > **PO** > **PE** > **PH**. The CP-corrected attraction energies in **PA** complexes are larger than those in **PO** ones. This term is 274.4 and 256.5 kcal mol^{-1} for $(NH_2)_3PO$ and Me_3PO in La^{3+} complexes, that is in accordance with the optimized metal–ligand distances (Table 2). Table 7 shows BSSE ($\Delta E_{CP-corrected} - \Delta E_{uncorrected}$) for Me/$NH_2$/OH/F complexes of La^{3+}. These with values of −25.7, −44.6, −37.5 and −13.6 kcal mol^{-1}, are relatively large. The difference between the uncorrected and CP-corrected ΔE is mainly related to the deformation energy. BSSE becomes negligible when the deformation term is added to $\Delta E_{CP-corrected}$. Equation 4 is able to describe well the calculated interaction energies for our systems, in which the deformation energies of subunits are added to $\Delta E_{CP-corrected}$. $\Delta E_{deformation}$ is zero for M because it is an atomic species. Table 7 shows that the deformation energies of $(NH_2)_3PO$ (49.7 kcal mol^{-1}) is about two times of that of Me_3PO (28.6 kcal mol^{-1}). Generally, large deformation of the ligand may imply a stronger metal–ligand interaction [55]. Thus, $(NH_2)_3PO$ is expected to establish the stronger non-covalent interaction, when compared with Me_3PO. But, the exothermic **L**···Ln^{3+} binding process supports the required energy for deformation of **L**. Therefore, $(NH_2)_3PO$ has less complete CP-corrected attraction energy ($-\Delta E_{GCP}$) than Me_3PO (by about 3 kcal mol^{-1}), because the former is more deformable. As shown in Table 7, the complete CP-corrected attraction energy ($-\Delta E_{GCP}$) decreases slightly from 227.8 in Me_3P = O–La^{3+} to 224.7 kcal mol^{-1} in $(NH_2)_3PO$–La^{3+} and drops markedly to 191.2 and 126.2 kcal mol^{-1} for corresponding $(OH)_3PO$ and F_3PO complexes, respectively, in line with decrease of dipole moment of ligands (Tables 1 and 7). These trends are observed for CH_2Me analogues as well as for Eu^{3+} and Lu^{3+} cations. In summary, interaction energies of **PA**s with lanthanide cations are very close to those of **PO**s.

Fully dissociation process of complexes is followed by two steps:

(i) The breaking of the **L′**–M^{3+} bond (when **L′** is deformed **L** in complex coordinate), that needs to the bond energy ($\Delta E_{bonding}$). The **L′**–M^{3+} bond energy is estimated by Eq 5, in which subunits have deformed geometry in complex coordinate with energies of $E^{ML}_{ML}(L)$ and $E^{ML}_{ML}(M)$. Indeed, the **L′**–M^{3+} bond energy is equal to $-\Delta E_{CP-corrected}$.

$$\Delta E_{bonding} = E^{ML}_{ML}(L) + E^{ML}_{ML}(M) - E^{ML}_{ML}(ML) \quad (5)$$

(ii) The geometry relaxation of separated **L′** to the parent free ligand **L**, which releases relaxation energy ($\Delta E_{relaxation} = -\Delta E_{deformation}$).

Fully dissociation process is the result of two aforementioned steps ($\Delta E_{diss} = \Delta E_{bonding} + \Delta E_{relaxation} = -\Delta E_{CP-corrected} - \Delta E_{deformation} = -\Delta E_{GCP}$). Table 7 shows that the $(NH_2)_3PO$–La^{3+} bond energy is larger than that in Me_3PO–La^{3+} (by about 18 kcal mol^{-1}). This is in good agreement with optimized O_P···La^{3+} distances (Table 2) and data of AIM analysis (Table 4). This phenomenon is intensified by increase of the electron donation ability of ligands as well as increase of the cation hardness. It can be concluded that the O_P–Ln^{3+} bond strength increase in the order of **PH** < **PE** < **PO** < **PA**. Fully dissociation energies of the complexes are calculated by consideration of the

Table 7 Interaction energies ΔE (kcal mol^{-1}) in the $\mathbf{LM}^{3+}$ complexes calculated with 6–311 ++ G** basis set at B3LYP, MP2 and CCSD(T) levels

Ligand	$\Delta E_{deformation} = -\Delta E_{relaxation}$ B3LYP/MP2/CCSD(T)	$\Delta E_{uncorrected}$ B3LYP/MP2/CCSD(T)	$\Delta E_{CP\text{-}corrected} = -\Delta E_{Bonding}$ B3LYP/MP2/CCSD(T)	$\Delta E_{GCP} = -\Delta E_{Diss}$ B3LYP/MP2/CCSD(T)
La^{3+}				
Me_3PO	28.6/31.1/29.7	−230.7/−234.2/−233.2	−256.5/−246.6/−243.3	−227.8/−215.4/−213.6
$(NH_2)_3PO$	49.7/53.8/52.2	−229.7/−238.5/−238.4	−274.4/−265.6/−262.2	−224.7/−211.7/−210.1
$(OH)_3PO$	46.7/49.0/49.4	−200.5/−214.7/−216.3	−238.0/−228.5/−228.9	−191.2/−179.4/−179.5
F_3PO	26.2/25.4/26.1	−138.8/−158.4/−161.2	−152.4/−144.0/−145.3	−126.2/−118.6/−119.2
$(CH_2Me)_3PO$	29.6/32.9/30.4	−248.8/−254.1/−252.9	−275.6/−266.2/−264.4	−246.0/−233.2/−233.9
$(NHMe)_3PO$	55.8/62.6/58.2	−249.5/−260.6/−259.6	−300.3/−294.0/−293.3	−244.5/−231.4/−232.2
$(OMe)_3PO$	59.4/62.4/63.8	−233.1/−249.1/−250.5	−283.1/−272.6/−274.9	−223.7/−210.3/−211.1
Cl_3PO	32.1/33.7/31.8	−178.6/−208.0/−212.3	−201.3/−194.8/−193.3	−169.2/−161.1/−161.6
Eu^{3+}				
Me_3PO	31.7/34.5/32.8	−254.1/−256.6/−255.8	−283.1/−272.2/−268.8	−251.4/−237.7/−236.0
$(NH_2)_3PO$	55.3/60.5/58.0	−254.0/−261.9/−261.5	−304.0/−295.0/−290.7	−248.6/−234.5/−232.7
$(OH)_3PO$	51.7/54.3/54.6	−222.6/−237.6/−238.3	−264.4/−254.9/−254.0	−212.7/−200.5/−199.4
F_3PO	30.1/29.5/30.1	−156.4/−178.4/−180.5	−173.0/−165.1/−165.6	−142.9/−135.6/−135.5
$(CH_2Me)_3PO$	32.8/36.5/33.7	−273.3/−277.4/−276.4	−303.5/−292.7/−290.9	−270.7/−256.2/−257.3
$(NHMe)_3PO$	62.8/77.1/65.4	−275.2/−284.4/−284.5	−332.8/−331.4/−321.8	−269.9/−254.3/−256.4
$(OMe)_3PO$	65.1/70.1/69.8	−257.7/−274.3/−274.7	−313.0/−303.7/−304.3	−247.9/−233.6/−234.5
Cl_3PO	36.1/38.5/35.9	−200.8/−229.2/−233.3	−227.0/−220.1/−217.8	−190.9/−181.6/−181.9
Lu^{3+}				
Me_3PO	33.7/35.9/34.8	−276.4/−276.7/−276.0	−307.6/−294.8/−292.2	−273.9/−258.9/−257.4
$(NH_2)_3PO$	58.8/63.2/61.6	−276.6/−283.3/−283.2	−330.1/−318.9/−315.8	−271.3/−255.7/−254.2
$(OH)_3PO$	55.0/57.5/58.0	−244.1/−257.4/−258.2	−288.9/−277.9/−281.8	−234.0/−220.5/−223.8
F_3PO	33.2/32.5/33.2	−174.8/−194.9/−197.8	−194.7/−184.6/−186.0	−161.5/−152.0/−152.8
$(CH_2Me)_3PO$	34.9/37.7/35.7	−296.3/−298.1/−297.7	−328.7/−315.9/−314.8	−293.8/−278.2/−279.1
$(NHMe)_3PO$	76.8/80.2/80.4	−298.5/−306.7/−306.6	−370.2/−356.7/−358.3	−293.4/−276.6/−277.9
$(OMe)_3PO$	69.7/73.1/74.8	−280.9/−295.4/−295.9	−340.8/−328.1/−331.2	−271.1/−255.0/−256.4
Cl_3PO	39.2/41.2/39.0	−220.8/−247.2/−252.9	−250.4/−241.2/−240.9	−211.2/−200.0/−201.9

relaxation energies. Table 7 shows that the value $|E_{relaxation}|$ in **PA** ligands is larger than that in **PO** ones. This causes the fully dissociation energies of complexes follow the sequence **PH** < **PE** < **PA** < **PO**.

Schurhammer et al. have previously compared the energy of optimized non-isoelectronic Me_3PO–La^{3+} and $(OMe)_3PO$–La^{3+} complexes at DFT/DZ* level. They have shown that the cation attraction energy decreases from 231.9 to 221.8 kcal mol^{-1} upon Me → OMe replacement [15]. We have obtained that the energy difference for aforementioned systems is 4.1 kcal mol^{-1} at B3LYP/6–311 ++ G** level. Moreover, it is found that the cation attraction energy decreases significantly from **PO**s to **PE**s when the isoelectronic ligands are compared. However, similar results in cation affinity can be found in both of two studies.

We have used MP2 and CCSD(T) methods to benchmark and validate the B3LYP values. Table 7 shows that the energy components calculated at MP2 are very close to those of CCSD(T). Moreover, DFT method overestimates the complete corrected attraction energies compared to MP2 and CCSD(T). The error obtained for B3LYP energies compared to MP2 and CCSD (T) values are about 7–17 kcal mol^{-1}. But, the trends in the metal–ligand interaction energies within the ligand series are stable when the computational level is changed.

3.5 Energy decomposition analysis (EDA)

The following interaction energy components can be obtained in the Morokuma analysis [45, 46]: (1) E_{elst}, the classical columbic interaction of the occupied orbitals (occ) of one fragment (A) with those of another fragment (B), (2) $E_{exch\text{-}rep}$, the exchange-repulsion energy arising from the Pauli exclusion which causes electron exchange between the occ(A) and occ(B); (3) E_{pol}, the polarization interaction which causes the mixing of occ and virtual orbitals (vir) within each fragment; (4) E_{CT}, the charge transfer

interaction which causes the interfragment delocalization by mixing occ of one fragment with vir of another and vice versa; (5) MIX, the remaining term in the interaction energy. For strong interactions, the higher order coupling term MIX usually becomes large in magnitude. Therefore, a modified scheme may be given by the sum of following terms:

$$E_{int}(\text{Hartree} - \text{Fock}) = E_{elst} + E_{exch-rep} + E_{CTPLX(A\rightarrow B)} + E_{CTPLX(B\rightarrow A)} + R$$

where $E_{CTPLX(A\rightarrow B)}$ is "the donative interaction", $E_{CTPLX(B\rightarrow A)}$ is "the back-donative interaction" and R is the higher-order coupling term. However, in the Morokuma approach, the total energy and its components are not free of BSSE. Hence, BSSE corrections were considered for calculation of the components and HF energies.

Table 8 collects the BSSE corrected $O_P\cdots Ln^{3+}$ energy decomposition analysis for the various complexes. The complete scheme is based on the Morokuma analysis [45, 46] in which the total interaction energy is decomposed into the electrostatic attraction (E_{elst}), exchange-repulsion ($E_{exch-rep}$), and the charge-transfer terms from ligand to metal, $E_{CTPLX(L\rightarrow M)}$, and from metal to ligand, $E_{CTPLX(M\rightarrow L)}$. The last two terms provide qualitative information on the extent of donated charge from the ligands to the metal and back-donated charges from the metal to the ligand. Our results reveal that the electrostatic term represents the largest contribution to the total interaction energy for the three systems La^{3+}, Eu^{3+}, and Lu^{3+}. The total HF interaction energy between the Ln^{3+} cations and the ligands clearly underestimate the DFT and MP2 bond dissociation energies, but the trends between the different systems remain the same. The EDA values for the electrostatic, exchange-repulsion and charge-transfer terms show markedly monotonic rules from La^{3+} to Lu^{3+} and are similar to the trend observed for binding energies and AIM results. Moreover, the absolute values of EDA terms change remarkably for the different ligands. The EDA data indicate that there is a significant contribution of the charge-transfer from ligand to metal and donative interaction increases in order **PH** < **PO** < **PE** < **PA**. The calculations show that $E_{CTPLX(M\rightarrow L)}$ amounts to 20–32% of the total attractive forces. It becomes obvious that the π back-donation interaction is, in all complexes, slightly

Table 8 Calculated EDA components (in kcal/mol) of La^{3+}, Eu^{3+} and Lu^{3+} complexes

Metal	Ligand	E_{elst}	$E_{exch-rep}$	$E_{CTPLX(L\rightarrow M)}$	$E_{CTPLX(M\rightarrow L)}$	HF energy
La^{3+}	Me_3PO	−197.99	119.71	−103.76	−64.36	−235.94
	$(NH_2)_3PO$	−225.45	124.47	−99.21	−67.87	−255.11
	$(OH)_3PO$	−204.60	97.81	−83.510	−53.66	−224.60
	F_3PO	−117.71	74.05	−65.87	−36.10	−136.84
	$(CH_2Me)_3PO$	−203.35	126.98	−117.55	−110.70	−252.24
	$(NHMe)_3PO$	−234.18	135.84	−115.24	−108.67	−276.32
	$(OMe)_3PO$	−238.32	115.42	−102.46	−64.78	−269.68
	Cl_3PO	−140.97	96.61	−96.22	−57.09	−182.12
Eu^{3+}	Me_3PO	−208.03	120.00	−109.58	−69.75	−260.54
	$(NH_2)_3PO$	−239.09	125.73	−105.84	−73.62	−277.64
	$(OH)_3PO$	−217.22	105.33	−76.49	−70.77	−240.02
	F_3PO	−128.44	77.96	−72.70	−41.63	−152.19
	$(CH_2Me)_3PO$	−210.41	149.26	−120.04	−114.20	−276.55
	$(NHMe)_3PO$	−244.19	136.44	−126.71	−123.55	−295.30
	$(OMe)_3PO$	−253.08	117.20	−110.27	−72.08	−280.76
	Cl_3PO	−148.85	98.16	−104.68	−70.76	−200.08
Lu^{3+}	Me_3PO	−216.02	120.80	−117.06	−74.39	−286.30
	$(NH_2)_3PO$	−248.72	126.84	−111.61	−78.00	−310.21
	$(OH)_3PO$	−229.12	108.76	−94.76	−81.91	−274.99
	F_3PO	−136.67	81.77	−79.28	−46.67	−177.22
	$(CH_2Me)_3PO$	−220.34	156.33	−131.05	−119.16	−304.66
	$(NHMe)_3PO$	−262.09	137.23	−131.56	−126.99	−346.02
	$(OMe)_3PO$	−251.74	119.39	−118.84	−79.94	−291.90
	Cl_3PO	−156.54	100.88	−112.59	−83.05	−229.09

smaller than the $E_{CTPLX(L\rightarrow M)}$. The largest π contribution is found for the $(NHMe)_3P=O$ ligand where the $Ln^{3+}\rightarrow O=P$ π back-donation has 26% of the total attractive energy (Table 8).

The data collected in Table 8 show that the electrostatic term yields 47.11–59.86%, 45.90–60.59% and 44.45–56.74% of the total attractive forces from La^{3+} to Lu^{3+}, respectively. Therefore, the metal–ligand bonding in Ln^{3+} complexes has a significant ionic character, especially in La^{3+} species. The conclusion is that the $Cl_3P=O$ ligand has the largest percentage of covalent character and thus the lowest percentage ionic character among the studied systems (47.11, 45.90, 44.45% for La^{3+}, Eu^{3+} and Lu^{3+}, respectively).

4 Conclusions

The electron donating ability of phosphoramides is more than that of their corresponding isoelectronic phosphoryl donors. Analysis of the natural charge of the cation revealed that the degree of LMCT in **PA** complexes is higher than that in the others. The NBO and AIM analyses show the strongest metal–ligand interaction in **PA** complexes. Comparison of the optimized structural parameters and estimated **L**–Ln^{3+} bond energies revealed that the **PA**$\cdots Ln^{3+}$ contacts are stronger than those of **PO**, **PE** and **PH** ones. The CP-corrected attraction energies follow the sequence of **PH** < **PE** < **PO** < **PA**, while the complete corrected attraction energies ($-\Delta E_{GCP}$) change as **PH** < **PE** < **PA** < **PO**, in which the deformation energies are considered. The fact that **PA**s are more deformable than **PO**s agrees with the previous different trends, which is confirmed by NBO and AIM analyses. The EDA data indicate that there is a significant contribution of the charge-transfer from ligand to metal and $E_{CTPLX(M\rightarrow L)}$ amounts to 20–32% of the total attractive forces. Moreover, donative interaction increases in order **PH** < **PE** < **PO** < **PA**, and the largest π contribution is found for the $(NHMe)_3P=O$ ligand. This is in good agreement with the calculated binding energies, AIM and NBO results. The energy components of the model systems calculated at DFT level relatively differ from the MP2 and CCSD(T) values, but trends in the metal–ligand interaction energies are independent of the computational level. The attraction energies of **PO** complexes are slightly more than those of **PA** ones (by about 2 to 3 kcal mol^{-1}). However, cation affinity of phosphoramides is very close to that of phosphine oxides and drops markedly in the cases of phosphates and phosphoryl trihalides. It can be concluded that phosphoramides are able to compete with phosphine oxides for lanthanide complexation from the energy point of view. Thus, taking into account that the synthesis pathway of phosphoramides is relatively inexpensive, they can be considered as efficient extracting agents.

Acknowledgment Support of this work by Tarbiat Modares University is gratefully acknowledged. We thank also Dr. Afshin Abbasi for his comments and helpful discussions.

References

1. Horwitz EP, Kalina DG, Diamond H, Vandegrift GF, Schulz WW (1985) Solvent Extr Ion Exch 3:75–109
2. Nash KL (1993) Solvent Extr Ion Exch 11:729–768
3. Bhattacharyya A, Mohapatra PK, Manchanda VK (2006) Solvent Extr Ion Exch 24:1–17
4. Modolo G, Nabet S (2005) Solvent Extr Ion Exch 23:359–373
5. Pierce TB, Peck PF (1963) Analyst 88:217–221
6. Yaftian MR, Burgard M, Matt D, Dieleman CB, Rastegar F (1997) Solvent Extr Ion Exch 15(6):975–989
7. Boehme C, Wipff G (2001) Chem Eur J 7:1398–1407
8. Nazarenko AY, Baulin VE, Lamb JD, Volkova TA, Varnek AA, Wipff G (1999) Solvent Extr Ion Exch 17(3):495–523
9. Atamas L, Klimchuk O, Rudzevich V, Pirozhenko V, Kalchenko V, Smirnov I, Babain V, Efremova T, Varnek A, Wipff G, Arnaud-Neu F, Roch M, Saadioui M, Bohmer V (2002) J Supramol Chem 2:421–427
10. Jenkins AL, Uy OM, Murray GM (1999) Anal Chem 71:373–378
11. Alexander V (1995) Chem Rev 95:273–342
12. Dam HH, Beijleveld H, Reinhoudt DN, Verboom W (2008) J Am Chem Soc 130:5542–5551
13. Berny F, Muzet N, Troxler L, Dedieu A, Wipff G (1999) Inorg Chem 38:1244–1252
14. Baaden M, Berny F, Boehme C, Muzet N, Schurhammer R, Wipff G (2000) J Alloys Compd 303–304:104–111
15. Schurhammer R, Erhart V, Troxler L, Wipff G (1999) J Chem Soc Perkin Trans 2:2423–2431
16. Troxler L, Hutschka DF, Wipff G (1998) J Mol Struct: THEOCHEM 431:151–163
17. Troxler L, Baaden M, Bohmer V, Wipff G (2000) Supramol Chem 12:27–51
18. Boehme C, Wipff G (2002) Inorg Chem 41:727–737
19. Chu IH, Zhang H, Dearden DV (1993) J Am Chem Soc 115:5736–5744
20. Staley RH, Beauchamp JL (1975) J Am Chem Soc 97:5920–5921
21. Hutschka F, Dedieu A, Troxler L, Wipff G (1998) J Phys Chem A 102:3773–3781
22. Pearson RG (1990) Coord Chem Rev 100:403–425
23. Hancock RD, Martell AE (1989) Chem Rev 89:1875–1914
24. Berny F, Wipff G (2001) J Chem Soc Perkin Trans 2:73–82
25. Modolo G, Odoj R (1999) Solvent Extr Ion Exch 17:33–53
26. Corbridge DEC (1995) Phosphorus: an outline of its chemistry, biochemistry and technology, 5th edn. Elsevier, Amsterdam
27. Wiberg E, Wiberg N, Holleman AF (2001) Inorganic chemistry. Academic Press, London, pp 613–614
28. Maron L, Eisenstein O (2000) J Phys Chem A 104:7140–7143
29. Cotton S (2006) Lanthanide and actinide chemistry. Wiley, Chichester
30. Dolg M, Stoll H, Savin A, Preuss H (1989) Theor Chim Acta 75:173–194
31. Dolg M, Stoll H, Savin A, Preuss H (1993) Theor Chim Acta 85:441–450
32. Ehlers AW, Bohme M, Dapprich S, Gobbi A, Hollwarth A, Jonas V, Kohler KF, Stegmann R, Veldkamp A, Frenking G (1993) Chem Phys Lett 208:111–114
33. Reed AE, Curtiss LA, Weinhold F (1988) Chem Rev 88:899–926

34. Bader RFW (1990) Atoms in molecules: A quantum theory. Oxford University Press, Oxford, UK
35. Bader RFW (1991) Chem Rev 91:893–928
36. Matta CF, Boyd RJ (2007) The Quantum Theory of Atoms in Molecules. WILEY-VCH Verlag GmbH & Co, KGaA, Weinheim
37. Rotzinger FP (2005) J Phys Chem B 109:1510–1527
38. Wahlin P, Danilo C, Vallet V, Real F, Flament JP, Wahlgren U (2008) J Chem Theory Comput 4:569–577
39. Torrent M, Gili P, Duran M, Sola M (1996) J Chem Phys 104:9499–9510
40. Dunbar RC (2002) J Phys Chem A 106:7328–7337
41. Fan HJ, Liu CW (1999) Chem Phys Lett 300:351–358
42. Chalasinski G, Szczesniak MM (1994) Chem Rev 94:1723–1765
43. Boys SF, Bernardi F (1970) Mol Phys 19:553–566
44. Frisch MJ, Trucks GW, Schlegel HB, Scuseria GE, Robb MA, Cheeseman JR, Zakrzewski VG, Montgomery JA Jr, Stratmann RE, Burant JC, Dapprich S, Millam JM, Daniels AD, Kudin KN, Strain MC, Farkas O, Tomasi J, Barone V, Cossi M, Cammi R, Mennucci B, Pomelli C, Adamo C, Clifford S, Ochterski J, Petersson GA, Ayala PY, Cui Q, Morokuma K, Malick DK, Rabuck AD, Raghavachari K, Foresman JB, Cioslowski J, Ortiz JV, Stefanov BB, Liu G, Liashenko A, Piskorz P, Komaromi I, Gomperts R, Martin RL, Fox DJ, Keith T, Al-Laham MA, Peng CY, Nanayakkara A, Gonzalez C, Challacombe M, Gill PMW, Johnson BG, Chen W, Wong MW, Andres JL, Head-Gordon M, Replogle ES, Pople JA (1998) Gaussian 98, revision A.7. Gaussian, Inc. Pittsburgh, PA
45. Kitaura K, Morokuma K (1976) Int J Quantum Chem 10:325–340
46. Morokuma K, Kitaura K (1981) Chemical applications of atomic and molecular electrostatic potentials. In: Politzer P, Truhlar DG (Eds). Plenum, New York
47. Schmidt MW, Baldridge KK, Boatz JA, Elbert ST, Gordon MS, Jensen JH, Koseki S, Matsunaga N, Nguyen KA, Su SJ, Windus TL, Dupuis M, Montgomery JA (1993) J Comput Chem 14:1347–1363
48. Gilheany DG (1994) Chem Rev 94:1339–1374
49. Dobado JA, Martinez-Garcia H, Molina JM, Sundberg MR (1998) J Am Chem Soc 120:8461–8471
50. Bollinger JC, Houriet R, Kern CW, Perret D, Weber J, Yvernault T (1985) J Am Chem Soc 107:5352–5358
51. Xantheas SS (1996) J Chem Phys 104:8821–8824
52. Jensen HB, Ross P (1969) Chem Phys Lett 3:140–143
53. Liu B, McLean AD (1973) J Chem Phys 59:4557–4558
54. Kim CK, Zhang H, Yoon SH, Won J, Lee MJ, Kim CK (2009) J Phys Chem A 113:513–519
55. Coupez B, Boehme C, Wipff G (2002) Phys Chem Chem Phys 4:5716–5729